Journal of Inflammation Research

Dovepress
Taylor & Francis Group

Open Access Full Text Article

ORIGINAL RESEARCH

MRPL35 Attenuates Neonatal Parenteral Nutrition-Associated Cholestasis by Modulating the ROS/JNK/NF-κB Pathway

Xiaodong Sun*, Leilei Shen*, Ruixue Zheng, Min Tao, Sheng Chen

Department of Pediatrics, The First Hospital Affiliated to Army Medical University, Chongqing, 400038, People's Republic of China

*These authors contributed equally to this work

Correspondence: Sheng Chen, Department of Pediatrics, The First Hospital Affiliated to Army Medical University, Chongqing, 400038, People's Republic of China, Tel +86-023-68766201, Email chensh129@tmmu.edu.cn

Objective: This study aimed to elucidate the role of the MRPL35/ROS/JNK/NF-κB signaling pathway in the pathogenesis of neonatal parenteral nutrition-associated cholestasis (PNAC) to identify underlying mechanisms and potential therapeutic targets.

Methods: The study employed both human and animal models. Neonates receiving parenteral nutrition for at least 2 weeks were divided into PNAC (n=10) and control groups (n=13). A PNAC model was established in male Sprague-Dawley rats (parenteral nutrition for 14 days, n=6/group), with interventions including adenovirus-mediated MRPL35 overexpression and N-acetylcysteine (NAC) treatment. Inflammatory markers, oxidative stress indicators, and signaling pathway activation were assessed using ELISA, immunohistochemistry, qRT-PCR, and Western blotting.

Results: Clinically, neonates with PNAC exhibited elevated serum levels of AST, DBil, TBA, TNF-α, and IL-1β, along with reduced levels of anti-inflammatory cytokines (IL-4, IL-10), increased ROS, and higher apoptosis in peripheral blood mononuclear cells (PBMCs). MRPL35 expression was significantly downregulated and JNK and NF-κB pathways were activated. In the animal model, PNAC rats showed severe liver injury, elevated TNF-α, IL-1β and ROS in hepatocytes, and higher hepatocyte apoptosis; the expression of *MRPL35* mRNA was significantly downregulated. Overexpression of MRPL35 reduced JNK/NF-κB activation, inflammatory cytokines, oxidative stress and liver injury, effects that were enhanced by co-treatment with N-acetylcysteine (NAC).

Conclusion: The MRPL35/ROS/JNK/NF-κB signaling pathway plays a critical role in the pathogenesis of PNAC. Targeting MRPL35 is expected to alleviate liver injury by blocking mitochondrial ROS signaling, offering a novel precision treatment model targeting the mitochondrial-inflammation axis for PNAC.

Keywords: cholestasis, total parenteral nutrition, MRPL35, oxidative damage, inflammation, animal model

Introduction

Total parenteral nutrition (TPN) is a critical intervention for neonates unable to tolerate enteral nutrition, such as premature infants and those with severe intestinal disease.[1,2] The incidence of PNAC ranges from 15–40% in neonates receiving TPN for more than 2 weeks, with higher risks in extremely low birth weight infants and those with intestinal failure.[3] Prolonged TPN use can lead to liver injury and metabolic disturbances.[3] Among these complications, parenteral nutrition-associated cholestasis (PNAC) is both common and severe, characterized by impaired bile flow and liver injury that can potentially progress to hepatic fibrosis and ultimately liver failure.[4] However, the pathogenesis of PNAC is complex and remains poorly understood. Therefore, elucidating the pathogenesis of PNAC is essential for developing effective preventive and therapeutic strategies.

Recent mechanistic studies have identified inflammation as the pivotal pathogenic driver of PNAC. El Kasmi et al demonstrated that activated hepatic macrophages secrete IL-1β, triggering NF-κB signaling pathway activation.[5,6] This inflammatory signaling disrupts hepatic homeostasis by transcriptionally suppressing two master regulators—LRH-1, which controls bile acid synthesis via *Cyp7a1* regulation,[7] and FXR (*Nr1h4*), which governs expression of canalicular

Received: 22 May 2025
Accepted: 21 September 2025
Published: 30 September 2025

transporters BSEP (*ABCB11*), MRP2 (*ABCC2*), and sterol exporters *ABCG5/8*.[5,6] The resulting impairment in bile acid synthesis and hepatocellular export capacity leads to intrahepatic accumulation of cytotoxic bile acids and phytosterols, culminating in cholestatic liver injury. These findings establish PNAC as a prototypical inflammation-mediated cholestatic disorder.

Notably, oxidative stress serves as both a trigger and amplifier of this inflammatory cascade in PNAC. The overproduction of reactive oxygen species (ROS) occurs through multiple mechanisms during parenteral nutrition, including mitochondrial dysfunction, NADPH oxidase activation, and lipid peroxidation from parenteral lipid emulsions, with neonates being particularly vulnerable due to their immature antioxidant systems. However, the specific molecular mechanisms through which ROS drives inflammatory activation in PNAC remain incompletely understood. Recent studies suggest that mitochondrial ribosomal protein L35 (MRPL35) may be a key molecular mediator of this oxidative-inflammatory axis. MRPL35, essential for oxidative phosphorylation complex assembly, directly regulates mitochondrial ROS production.[8,9] MRPL35 downregulation triggers excessive ROS production, mitochondrial damage, and subsequent release of mitochondrial DNA (mtDNA).[10,11] This released mtDNA activates the AIM2 inflammasome, promoting IL-1β secretion and perpetuating inflammatory responses.[12] Thus, the MRPL35-mediated regulation of the ROS/JNK/NF-κB pathway may be a core mechanism through which oxidative stress drives inflammatory activation in PNAC. While MRPL35 has been implicated in various malignant diseases, its role in PNAC remains unexplored.

Based on this evidence, we hypothesize that downregulation of MRPL35 exacerbates PNAC through the ROS/JNK/NF-κB pathway. In this study, we aim to elucidate these underlying pathogenic mechanisms and identify potential therapeutic targets.

Materials and Methods

Human Peripheral Blood

This prospective study included neonates admitted to the neonatal intensive care unit (NICU) of the Southwest Hospital of Third Military Medical University, China, between August 2021 and February 2022. Eligibility criteria required neonates to have received parenteral nutrition (PN) for at least two weeks. The diagnosis of PNAC was made in accordance with established criteria from the literature,[2,13,14] defining the condition in patients receiving PN for more than two weeks with without other identifiable causes of cholestasis, and characterized by a serum direct (conjugated) bilirubin level exceeding 2 mg/dL (34.2 μmol/L) or accounting for more than 20% of the total bilirubin. Based on these criteria, 10 neonates were enrolled in the PNAC group, while 13 neonates who received PN but did not develop cholestasis served as the control group. There were no statistically significant differences between the two groups regarding gestational age, sex, birth weight, or the duration of PN administration (Table 1). Peripheral blood samples were collected from all participants for subsequent analysis.

This study was conducted in accordance with the Declaration of Helsinki and the ethical guidelines outlined in the Belmont Report. The Institutional Ethics Review Board of the Southwest Hospital of Third Military Medical University approved the study protocol (approval number: KY2021050). Written informed consent was obtained from the parents or legal guardians of all enrolled neonates.

Table 1 Comparison of Clinical Data Between the Two Groups

Basic Characteristics	Control (n=13)	PNAC (n=10)	*P*	F
GA (w)	30.28±2.92	30.01±3.89	0.848	0.72
BW (Kg)	1.30±0.43	1.31±0.49	0.987	0.001
Male (%)	7 (53.8%)	8 (80%)	0.197	6.251
Duration of Parenteral Nutrition (d)	20.15±5.91	21.4±5.56	0.365	0.07

Abbreviations: GA, Gestational age; BW, Birth weight; w, week; d, day.

Experimental Animals

Male Sprague-Dawley rats, aged 6–8 weeks and weighing 220–240 g, were obtained from the Third Military Medical University (Chongqing, China). All animal experiments were approved by the Laboratory Animal Welfare and Ethics Committee of Army Medical University (approval number: AMUWEC20201551) and adhered to the NIH Guide for the Care and Use of Laboratory Animals. The rats were housed under controlled conditions (23°C, 40%-60% humidity, 12-hour light/dark cycle) with free access to standard rat chow and water.

To investigate the MRPL35/ROS/JNK/NF-κB pathway's role in PNAC, 18 rats were randomly divided into three groups (n=6/group): control, sham surgery, and PNAC. The dietary solution was formulated following Hodin et al's method,[15] providing 205 kcal/kg/day. Each liter of the solution contained the following components: 450 mL of amino acid mixture (Sinopharm Double-Crane Pharmaceutical), 360 mL of 50% glucose (Otsuka Pharmaceutical), and 140 mL of lipid emulsion (SMOFlipid; Fresenius Kabi). Additionally, the solution was supplemented with electrolytes (Adamel; Fresenius Kabi), trace elements (Adamel; Fresenius Kabi), lipid-soluble vitamins (Vitintra; Fresenius Kabi), and water-soluble vitamins (Soluvit; Fresenius Kabi). Rats in the control group were not catheterized and had free access to food and water. Rats in the sham-operated group were catheterized via the right jugular vein and infused with saline (1 mL/h for the first 24 h, then 2 mL/h) while maintaining access to food and water. Rats in the PNAC group were catheterized via the right jugular vein and continuously infused with TPN solution (1 mL/h for the first 24 hours, then 2 mL/h) with food and water deprivation. After 14 days, animals were euthanized by intraperitoneal injection of pentobarbital at a dose of 150–200 mg/kg.[16] Peripheral blood and liver tissue samples were subsequently collected.

To investigate the therapeutic potential of MRPL35 overexpression ($MRPL35^{+}$), Adenovirus was administered one week before the start of the experiment. 24 rats were randomly divided into four groups (n=6/group): PNAC, PNAC + empty adenovirus (Ad-null), PNAC+$MRPL35^{+}$, and PNAC+$MRPL35^{+}$+ N-acetylcysteine (NAC) (PNAC+$MRPL35^{+}$ +NAC). All groups were subjected to jugular vein catheterization. Prior to catheterization, the PNAC + Ad-null group received a tail vein injection of 10 μL of 1×10^{11} PFU/mL empty adenovirus; the $MRPL35^{+}$ group received 10 μL of 1×10^{11} PFU/mL MRPL35 overexpression adenovirus; and the $MRPL35^{+}$+NAC group received the same dose of adenovirus plus 150 mg/kg NAC added to the TPN solution. On the 14th day, all rats were euthanized via intraperitoneal injection of pentobarbital at a dose of 150–200 mg/kg,[16] and blood and liver tissue samples were collected.

Detection of Inflammatory Factors and Markers of Oxidative Stress

Enzyme-linked immunosorbent assay (ELISA) was used to quantify inflammatory cytokines (TNF-α, IL-1β, IL-10, IL-4) in both human and rat samples. For rat samples, cytokines were measured in liver tissue and plasma. Oxidative stress markers, including malondialdehyde (MDA), hydroxyl radical scavenging ability, superoxide dismutase (SOD), and glutathione peroxidase (GSH-Px), were assessed in plasma samples from both neonates and rats using chemical reagent methods. All procedures were performed according to the kit instructions (Table S1). The optical density of each well was determined at a wavelength of 450 nm using a microplate reader. After obtaining the optical density value for each sample, the corresponding cytokine concentration was calculated based on the standard curve.

Immunohistochemistry

Paraffin-embedded liver sections were deparaffinized and rehydrated. Antigen retrieval was performed by boiling in citrate buffer for 15 minutes. Sections were treated with peroxidase inhibitor, blocked with goat serum, and incubated with primary TNF-α antibody (1:20) overnight. After washing, secondary antibody (1:100) was applied (Table S1), followed by HRP and DAB for visualization. Hematoxylin counterstaining was performed before microscopic examination. Quantitative analysis was performed by counting TNF-α positive cells in 10 random high-power fields (400×) per sample using ImageJ software. Results were expressed as positive cells per high-power field.

DCFH-DA Fluorescent Probe

The expression of ROS was measured using the DCFH-DA fluorescent probe assay kit. Liver tissue was ground in liquid nitrogen, suspended in lysis buffer, and homogenized. The homogenate was filtered through a 100–200 μm mesh filter

and centrifuged to collect the cell pellet. The pellet was washed twice with PBS, resuspended in a 10 μM probe solution (diluted 1:1000 in PBS), and incubated at 37°C for 1 hour with intermittent mixing. After incubation, the sample was centrifuged to collect the pellet, which was then used for slide preparation and FITC fluorescence imaging (Table S1). Fluorescence intensity was quantified using ImageJ software, measuring mean fluorescence intensity (MFI) in at least 100 cells per sample. Results were normalized to control group values.

Peripheral Blood Mononuclear Cell (PBMC) Isolation

PBMC isolation was performed using density gradient centrifugation as follows: Dilution: Peripheral whole blood was mixed 1:1 (v/v) with phosphate-buffered saline (PBS). Layering: An appropriate volume of separation medium was dispensed into a sterile centrifuge tube; the diluted blood was carefully layered on top to create a distinct interface. Centrifugation: 500–1000 × g for 20–30 min at room temperature. Stratification (top to bottom): (i) plasma layer; (ii) white, cloudy buffy-coat layer (PBMCs); (iii) separation medium layer; (iv) granulocyte + erythrocyte pellet. Collection: The PBMC layer was gently aspirated with a sterile pipette and transferred to a fresh 15 mL centrifuge tube. Wash: 10 mL cell-washing buffer was added, gently mixed, and centrifuged at 250 × g for 10 min; the supernatant was discarded. Resuspension: The pellet was resuspended in 5 mL cell-washing buffer, centrifuged at 250 × g for 10 min, and the supernatant discarded; this step was repeated once. Count and viability assessment: Cell number and viability were determined with an automated cell counter; only samples with ≥90% viability were used for downstream experiments.

Flow Cytometry

Before the experiment, the cell culture chamber and biosafety cabinet were sterilized with ultraviolet light for 30 minutes and cleaned with 75% ethanol. For liver cell isolation, the liver was perfused with 0.025% type IV collagenase solution at 37°C at 20 mL/min. The collected liver cells were transferred to 4°C DMEM, filtered through a mesh sieve, and centrifuged at 600 rpm for 5 minutes. This process was repeated three times to purify the cells, which were then placed on ice. For cell staining, 50,000 to 100,000 cells were centrifuged at 1000 rpm for 5 minutes, and the supernatant was discarded. The cell pellet was resuspended in 195 μL Annexin V-FITC binding buffer. Then, 5 μL Annexin V-FITC and 10 μL propidium iodide (PI) staining solution were added and gently mixed. The cells were incubated in the dark at room temperature (20–25°C) for 10–20 minutes, followed by an ice bath. Flow cytometric analysis was performed on a BD Flow Cytometer.

Immunofluorescence Labeling

PBMCs were isolated and fixed with 4% paraformaldehyde, then permeabilized with 0.5% Triton X-100 for 20 minutes. Cells were blocked with goat serum for 30 minutes at room temperature. The cells were then incubated with primary antibodies overnight at 4°C: MRPL35 (1:100, Affinity), p-JNK (1:50, Santa Cruz), and p-p65 (1:20, R&D Systems). After washing with PBS, the cells were incubated with fluorescent secondary antibodies (1:50) for 1 hour at 37°C. Finally, the cells were counterstained with DAPI (1:10,000) for 5 minutes and mounted with antifade medium.

Paraffin-embedded liver sections were deparaffinized and rehydrated. Antigen retrieval was performed by boiling the sections in citrate buffer for 15 minutes, followed by cooling and washing with PBS. Sections were then blocked and incubated with primary antibodies overnight at 4°C: MRPL35 (1:100), p-JNK (1:50), and p-p65 (1:20). Secondary antibodies (1:50) were applied for 1 hour at room temperature. Sections were counterstained with DAPI for 3 minutes, washed with PBS, and mounted with antifade medium. Fluorescence was observed with a fluorescence microscope (Table S2).

Real-Time Quantitative PCR (qRT-PCR)

Total RNA was extracted using Trizol reagent. RNA purity was assessed by measuring the OD260/OD280 ratio using a UV spectrophotometer. Complementary DNA (cDNA) was synthesized from the extracted RNA using ReverTra Ace-α reverse transcription kit. The reverse transcription conditions were as follows: 42°C for 10 minutes, 30°C for 20 minutes, 99°C for 5 minutes, and 4°C for 5 minutes. Quantitative real-time PCR (qRT-PCR) was performed using 2× SYBR Green Master Mix in a final reaction volume of 20 μL, which consisted of 10 μL SYBR Green, 2 μL cDNA template, 0.3 μL

forward primer, 0.3 μL reverse primer, and deionized water. GAPDH was used as an internal control. Relative expression levels of MRPL35 were determined by the comparative Ct method (Table S3).

Western Blotting

PBMCs were isolated from human and rat samples. Rat liver tissues were minced, ground to a fine powder with liquid nitrogen, and lysed on ice for 30 minutes. After centrifugation, the supernatant was collected and mixed with 5× loading buffer. Equal amounts of protein samples were subjected to electrophoresis and transferred to PVDF membranes. The membranes were blocked and incubated with primary antibodies at the following dilutions: rabbit anti-MRPL35 (1:500, Affinity DF3668), rabbit anti-p65 (1:500, Novus NB100-2176), rabbit anti-phospho-p65 (1:500, Novus NB100-82088), mouse anti-JNK (1:500, Santa Cruz sc-7345), mouse anti-phospho-JNK (1:500, Santa Cruz sc-6254), and mouse anti-β-actin (1:1000, Santa Cruz sc-47778) overnight at 4°C. The next day, the membranes were incubated with secondary antibodies for 2 hours at room temperature and visualized by chemiluminescence. Gray scale values were analyzed using ImageJ software, and protein expression levels were normalized to β-actin.

Hematoxylin and Eosin Staining

Sections (4–5 μm) were baked at 60°C for 30–60 min, deparaffinized in xylene (2× 5–10 min), and rehydrated through graded ethanols (100%, 5 min; 90%, 2 min; 70%, 2 min). Slides were stained with hematoxylin (3 min, room temperature), rinsed in PBS (1 min), differentiated in 1% HCl/ethanol (10 s), and washed again in PBS (1 min). Cytoplasm and collagen were counterstained with 1% eosin Y (20 s) and briefly rinsed in PBS (10 s). Dehydration was performed through ascending ethanols (95%, 5 min; 100%, 2×3 min), followed by clearing in xylene (2× 5 min). Coverslips were mounted using neutral balsam, and sections were examined under a light microscope.

Statistical Analysis

Statistical analyses were performed using SPSS 23.0 (IBM Corporation). Data were expressed as mean ± standard deviation. One-way ANOVA with LSD post hoc test was used for normally distributed data, while Kruskal–Wallis *H*-test with Dunnett's T3 post hoc test was used for non-parametric data. Sample size was calculated using G*Power 3.1 to achieve 80% power (α=0.05). Graphs were generated using GraphPad Prism 8.0 (GraphPad Software, La Jolla, CA, USA). Statistical significance: $*P < 0.05$, $**P < 0.01$, $***P < 0.001$.

Results

Clinical Evaluation of the MRPL35/ROS/JNK/NF-κB Pathway in Neonates with PNAC

Liver function indicators were compared between the two groups of newborns. There were no statistically significant differences in serum markers such as ALT, TBil, and GGT between the control and PNAC groups. However, serum levels of AST, DBil, and TBA were significantly elevated in the PNAC group compared with the control group (Table 2). The PNAC group also showed significant changes in inflammatory cytokines, with increased levels of TNF-α and IL-1β and decreased levels of anti-inflammatory cytokines IL-4 and IL-10 (Figure 1A). The apoptotic index in PBMCs was significantly higher in the PNAC group (Figure 1B), and ROS expression in mononuclear cells was significantly increased (Figure 1C). Oxidative stress markers, including MDA, SOD, GSH-Px, and hydroxyl radical scavenging ability, showed significant differences between the groups, with increased MDA levels and compensatory increases in SOD, GSH-Px, and hydroxyl radical scavenging ability in the PNAC group (Figure 1D). MRPL35 mRNA expression was significantly downregulated in the PNAC group (Figure 1E). Protein levels of JNK and NF-κB pathway components were significantly upregulated, with phosphorylated forms of JNK and the p65 subunit of NF-κB showing higher levels (Figure 1F). Fluorescence staining of MRPL35 and phosphorylated JNK (p-JNK) and phosphorylated NF-κB (p-P65) in mononuclear cells confirmed these results and illustrated their cellular localization (Figure 1G).

Table 2 Comparison of Serum Liver Function Indexes Between the Two Groups

Group	n	ALT (U/L)	AST (U/L)	GGT (U/L)	TBA (μmol/L)	TBiL (μmol/L)	DBiL (μmol/L)
Neonate							
Control	13	9.25±8.66	23.97±7.61	131.21±157.34	22.88±14.29	54.51±55.42	5.73±4.35
PNAC	10	22.57±24.35	62.93±49.72*	206.88±158.6	47.14±18.01*	88.99±48.09	38.11±27.43*
F		3.480	9.034	0.550	1.326	0.074	13.834
P		0.08	0.036	0.267	0.002	0.133	0.005
Rat							
Control	6	18.23±8.48	53.28±10.10	0.65±0.21	6.83±1.89	2.15±0.39	0.43±0.10
Sham	6	25.78±5.85	74.93±1.24	0.58±0.26	6.38±1.81	2.03±0.48	0.38±0.10
PNAC	6	46.13±10.03*	286.53±117.08*	13.33±7.06*	24.83±5.33*	5.40±1.54*	1.03±0.43*
PNAC + Ad-null	6	48.10±11.23	286.75±43.79	20.68±1.84	32.83±5.78	3.93±2.11	2.25±2.88
PNAC+ MRPL35^{+}	6	33.80±3.75	120.35±6.68	5.45±0.51	15.35±3.32	3.53±1.42	0.93±0.24
PNAC+ MRPL35^{+}+NAC	6	17.70±2.96	65.88±6.81	1.20±1.07	5.33±1.10	3.15±1.49	0.85±0.70
H		19.969	21.209	19.791	19.991	10.266	11.235
P		0.001	0.001	0.001	0.001	0.068	0.047

Note: *$P<0.05$.
Abbreviations: ALT, Alanine aminotransferase; AST, Aspartate aminotransferase; GGT, Transglutaminase; TBA, Total bile acids; TBiL, Total bilirubin; DBiL, Direct bilirubin.

Assessment of the MRPL35/ROS/JNK/NF-κB Pathway in a PNAC Animal Model

Table 2 presents liver function data indicating the successful establishment of our PNAC animal model. The PNAC group showed significantly elevated hepatic levels of TNF-α and IL-1β (Figure 2A). Histopathological examination revealed severe liver injury in the PNAC group, characterized by extensive hepatocyte necrosis and hepatocyte vacuolization, disrupted lobular architecture, disorganized hepatocyte arrangement, and numerous pseudolobules, which was more pronounced than in the control and sham-operated groups (Figure 2B and Figure S1). Immunohistochemical staining for TNF-α showed a significantly stronger signal in the liver tissues of the PNAC group, and the mean optical density value increased significantly (Figure 2C and Figure S2). Flow cytometry analysis revealed a significant increase in the apoptotic index of hepatocytes in the PNAC group (Figure 2D). ROS expression levels in hepatocytes were significantly higher in the PNAC group (Figure 2E). qRT-PCR analysis revealed a significant downregulation of MRPL35 mRNA expression in hepatocytes from the PNAC group (Figure 2F). Fluorescent staining of rat liver showed that the expression of MRPL35 was attenuated in the PNAC group, while the expression of JNK and NF-κB phosphorylated forms was increased (Figure 2G).

Effects of MRPL35 Overexpression on a PNAC Animal Model

To further investigate the role of the MRPL35/ROS/JNK/NF-κB pathway in PNAC, we conducted experiments involving MRPL35 overexpression and NAC treatment in a PNAC rat model. qRT-PCR analysis showed a pronounced downregulation of MRPL35 mRNA of rat liver in the PNAC group, which was effectively reversed by MRPL35 overexpression (Figure 3A). In the liver tissue of rats overexpressing MRPL35, with or without NAC treatment, Western blotting confirmed elevated MRPL35 protein levels and reduced p-JNK and p-p65 levels compared to the PNAC group (Figure 3B). Serum analysis indicated significantly elevated levels of TNF-α and IL-1β in the PNAC group, which were attenuated by MRPL35 overexpression and further reduced by NAC treatment (Figure 3C). Histopathological examination revealed severe liver injury in the PNAC group, characterized by extensive hepatocyte necrosis, increase in the number and percentage of vacuole area of hepatocytes, disrupted lobular architecture, and disorganized hepatocyte arrangement (Figure 3D and Figure S3). This damage was significantly more pronounced than that observed in the control and sham-operated groups (Figure 2B). Immunohistochemical analysis of rat liver showed intense TNF-α signaling and the mean optical density value increased

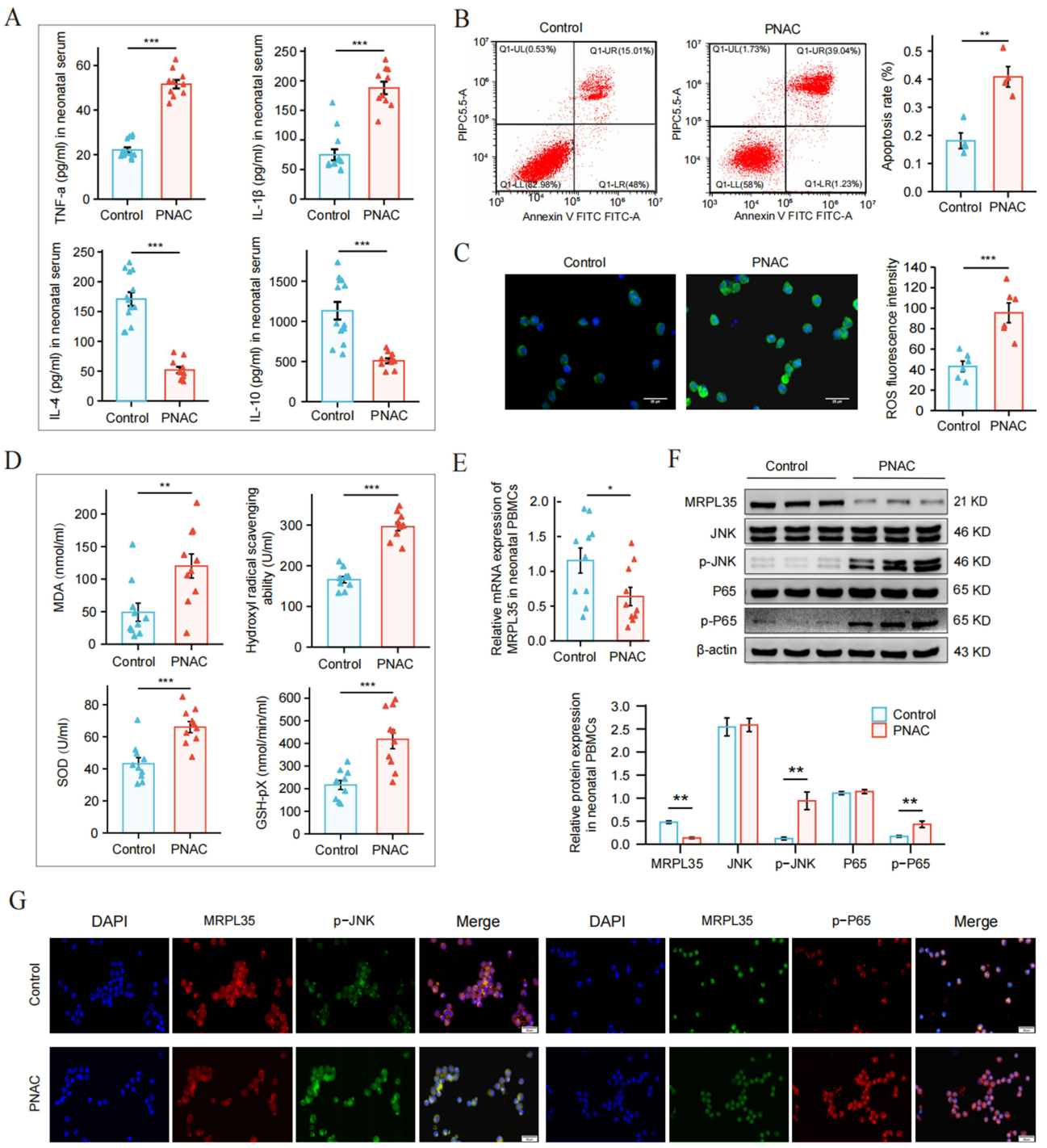

Figure 1 Clinical Evaluation of the MRPL35/ROS/JNK/NF-κB Pathway in Neonates with PNAC. (**A**) Serum levels of TNF-α, IL-1β, IL-4, and IL-10 in neonates. ***P<0.001. (**B**) Apoptosis of PBMCs determined by flow cytometry. **P<0.01. (**C**) Expression level of ROS in PBMCs was detected by immunofluorescence (×400). ***P<0.001. (**D**) Serum levels of MDA, Hydroxyl radical scavenging ability, SOD, and GSH-Px in neonates. **P<0.01, ***P<0.001. (**E**) Expression of MRPL35 mRNA in PBMCs was detected by qRT-PCR. Values are means ± SD. *P<0.05. (**F**) Representative Western blot images of MRPL35, JNK, p-JNK, P65 and p-P65 in neonatal PBMCs. Values are means ± SD from three experiments. **P<0.01. (**G**) Double immunofluorescence images for MRPL35 (red) + p-JNK (green) and MRPL35 (green) + p-P65 (red). DAPI staining (blue) indicates the nucleus. (scale bar =20 μm).

significantly in the PNAC and PNAC + Ad-null groups, significantly reduced by MRPL35 overexpression and further attenuated by NAC treatment (Figure 3E and Figure S4). Flow cytometry indicated a high apoptotic index of hepatocytes in the PNAC group, significantly decreased by MRPL35 overexpression and further reduced by NAC treatment (Figure 3F). ROS levels of hepatocytes were markedly elevated in the PNAC group but were significantly reduced by MRPL35

https://doi.org/10.2147/JIR.S528466

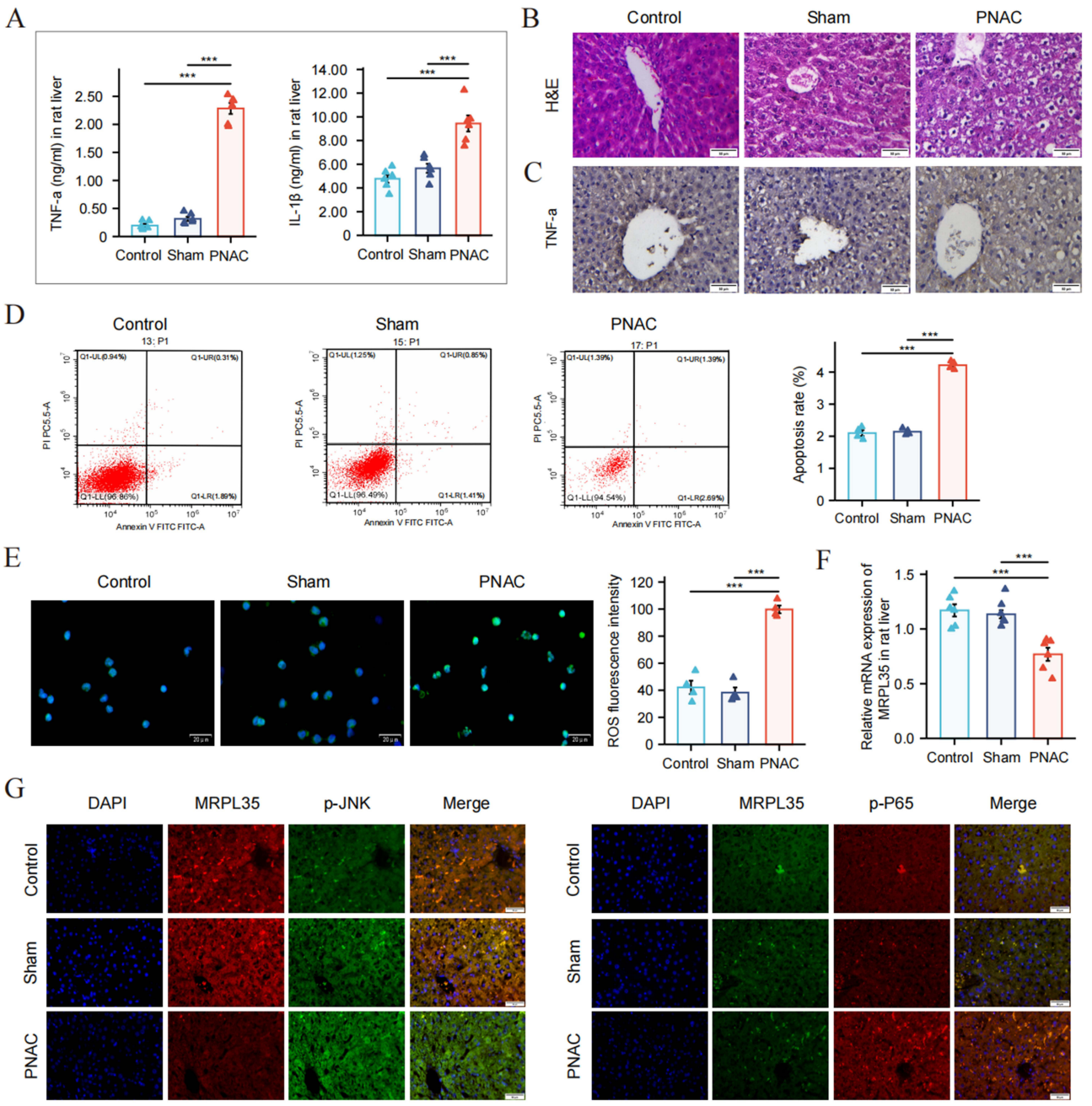

Figure 2 Assessment of the MRPL35/ROS/JNK/NF-κB Pathway in a PNAC Animal Model. (**A**) Levels of TNF-α and IL-1β in rat liver.***P<0.001. (**B**) Hematoxylin and eosin (H&E) staining of rat liver tissue (×200). (**C**) Immunohistochemical images of TNF-α in rat liver tissue (×200). (**D**) Apoptosis of hepatocytes was determined by flow cytometry. ***P<0.001. (**E**) Expression level of ROS in hepatocytes was detected by immunofluorescence (×400). ***P<0.001. (**F**) Expression of MRPL35 mRNA in rat liver detected by qRT-PCR. ***P<0.001. (**G**) Double immunofluorescence images for MRPL35 (red) + p-JNK (green) and MRPL35 (green) + p-P65 (red). DAPI staining (blue) represents the nucleus (scale bar =20 μm).

overexpression and further decreased by NAC treatment (Figure 3G). Biochemical assays revealed increased serum MDA levels in the PNAC group, reversed by MRPL35 overexpression and NAC treatment, along with decreased levels of SOD, GSH-Px, and hydroxyl radical scavenging activities (Figure 3H).

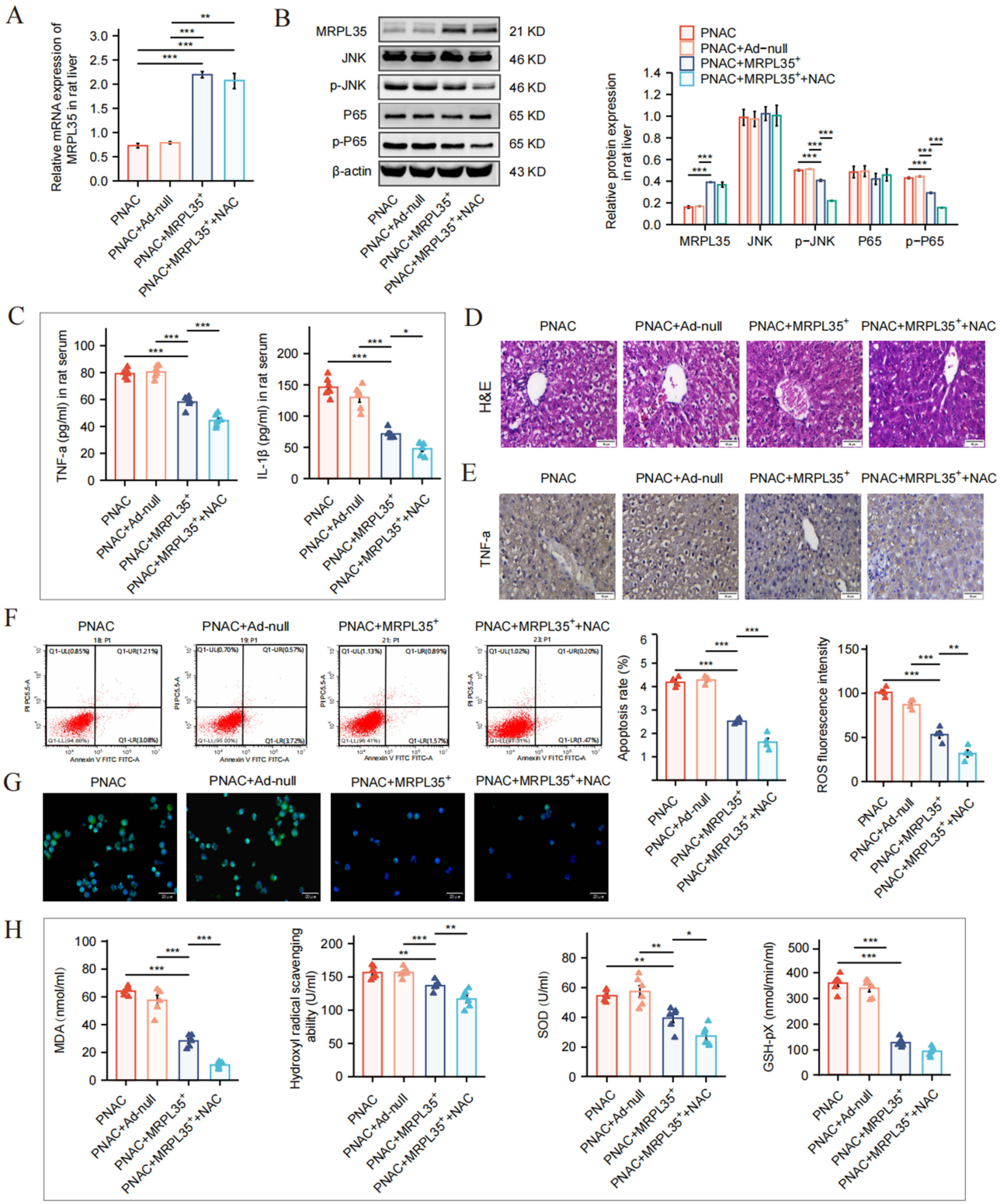

Figure 3 Effects of MRPL35 Overexpression on a PNAC Animal Model. (**A**) Expression of MRPL35 mRNA in rat liver detected by qRT-PCR.****P*<0.001,***P*<0.01. (**B**) Representative Western blot images of MRPL35, JNK, p-JNK, P65 and p-P65 in rat liver. Values are means ± SD from three experiments. ****P*<0.001. (**C**) Serum levels of TNF-α and IL-1β in rats.****P*<0.001,**P*<0.05. (**D**) Hematoxylin and eosin (H&E) staining of rat liver (×200). (**E**) Immunohistochemical image of TNF-α in rat liver (×200). (**F**) Apoptosis of hepatocytes determined by flow cytometry. ****P*<0.001. (**G**) Expression level of ROS in hepatocytes detected by immunofluorescence (×400). ****P*<0.001, ***P*<0.01. (**H**) Serum levels of MDA, Hydroxyl radical scavenging ability, SOD, and GSH-pX. ****P*<0.001, ***P*<0.01, **P*<0.05.

https://doi.org/10.2147/JIR.S528466

Discussion

Our study provides critical insights into the role of the MRPL35/ROS/JNK/NF-κB pathway in neonatal PNAC. To our knowledge, this is the first study to show MRPL35 downregulation in both clinical and animal models of PNAC, establishing a novel link between mitochondrial dysfunction and cholestatic liver injury during parenteral nutrition. The downregulation of MRPL35, essential for assembling oxidative phosphorylation complexes,[8,9] likely impairs mitochondrial function. This disruption leads to excessive ROS production that activates the JNK/NF-κB pathways, creating a vicious cycle of inflammation that perpetuates liver injury.

In our animal model, MRPL35 overexpression attenuated inflammation and oxidative stress. The concurrent reduction in antioxidant enzyme activity (SOD, GSH-Px) likely reflects a restoration of cellular redox homeostasis rather than a detrimental effect. By addressing the primary source of mitochondrial ROS, MRPL35 overexpression reduces the overall oxidative burden, thus lessening the need for a compensatory antioxidant response. This interpretation is supported by the simultaneous decrease in MDA levels and improved liver histology.

Our study builds on the paradigm of PNAC as an inflammation-driven disorder by identifying MRPL35 as an upstream regulator of the inflammatory cascade previously described by El Kasmi et al[5,6,17] The correlation between MRPL35 downregulation and NF-κB activation in our clinical samples suggests mitochondrial dysfunction is a primary trigger of inflammation in PNAC, not merely a secondary effect of liver injury. The mechanistic link likely involves several interconnected pathways. MRPL35 deficiency can impair mitochondrial protein synthesis, leading to increased ROS generation.[10,11] It may also trigger the release of damage-associated molecular patterns (DAMPs) like mtDNA following mitochondrial damage, a concept supported by our apoptosis data.[12] Finally, this increase in ROS can directly activate the JNK/NF-κB signaling pathway,[18,19] as shown in our results.

The therapeutic efficacy of combining MRPL35 overexpression with NAC treatment deserves special consideration. While MRPL35 overexpression alone significantly improved liver function and reduced inflammation, the addition of NAC provided synergistic benefits. This synergy suggests that targeting both the source of ROS (mitochondrial dysfunction) and the existing oxidative stress (through antioxidant supplementation) may be necessary for optimal therapeutic outcomes. This dual-targeting approach addresses both the upstream cause and downstream consequences of oxidative stress in PNAC, potentially offering a more comprehensive therapeutic strategy than either intervention alone.

The clinical implications of our findings extend beyond mechanistic insights. Current preventive strategies for PNAC primarily focus on optimizing parenteral nutrition composition, promoting enteral feeding, and using alternative lipid emulsions.[20] Our identification of MRPL35 as a key regulator suggests that mitochondrial-targeted therapies could represent a novel therapeutic avenue. Potential translational approaches might include: (1) screening for MRPL35 expression levels as a biomarker for PNAC risk stratification, (2) developing small molecules that stabilize MRPL35 or enhance its expression, (3) utilizing mitochondrial-targeted antioxidants that specifically address mitochondrial ROS, and (4) implementing combination therapies that simultaneously target mitochondrial function and inflammatory pathways.

It is noteworthy that MRPL35 has been previously implicated in various malignancies, where its upregulation promotes tumor progression.[21] The contrasting roles of MRPL35 in cancer versus PNAC highlight the context-dependent nature of mitochondrial protein function. In rapidly proliferating cancer cells, enhanced mitochondrial biogenesis supports increased energy demands and biosynthetic processes. Conversely, in the metabolically stressed hepatocytes of PNAC patients, MRPL35 deficiency disrupts normal mitochondrial function, leading to oxidative damage and inflammation. This dichotomy underscores the importance of understanding tissue-specific and disease-specific roles of mitochondrial proteins when developing targeted therapies.

Elemental nutrients in TPN can serve as significant sources of oxidants due to nutrient interactions, antioxidant/pro-oxidant imbalances, and environmental factors.[12] Neonates receiving TPN are particularly vulnerable to oxidative stress overload due to their immature antioxidant defenses. The combination of high lipid intake, the presence of plant sterols in lipid emulsions, and TPN-induced intestinal inflammation contributes to ROS production.[12,22] This leads to hepatocellular damage through lipid peroxidation and the formation of reactive aldehydes such as MDA.

The mitochondrial ribosomal protein (MRP) family plays an indispensable role in protein synthesis and mitochondrial function, orchestrating apoptosis, protein biosynthesis, and signal transduction.[23,24] MRPL35, a key mitochondrial ribosomal protein, is critical for the synthesis and assembly of the cytochrome c oxidase (COX) complex, a vital component of oxidative phosphorylation.[9,25] MRPL35 deficiency increases mitochondrial ROS, which in turn activates the pro-inflammatory JNK/NF-κB pathway. This finding provides a crucial upstream link to established mechanisms, as this inflammatory cascade is known to suppress key regulators of bile acid homeostasis like FXR and LRH-1.[26] We therefore speculate that the MRPL35 downregulation we observed is a critical initiating event that triggers this entire sequence, ultimately causing the intrahepatic bile acid accumulation that manifests as cholestasis.

Prior studies have shown that MRPL35 downregulation in colon cancer cells significantly increases ROS production, establishing a clear link between MRPL35 and ROS regulation. Building on this, we speculate that a similar mechanism occurs in PNAC: the downregulation of MRPL35 leads to excessive ROS production, which in turn triggers mitochondrial damage, mtDNA release, and the subsequent activation of inflammatory and innate immune responses that drive the disease. It has been reported that increased mitochondrial outer membrane permeabilization (MOMP) can lead to the release of intermembrane space proteins, the initiation of intrinsic apoptosis,[27] and the translocation of mtDNA into the cytoplasm, where it is recognized by cyclic guanosine monophosphate (GMP)-AMP synthase (cGAS) to activate the stimulator of interferon genes (STING) signaling pathway.[28,29] Additionally, studies have found that internalized bacterial endotoxin lipopolysaccharide (LPS) activates the pore-forming protein GasderminD (GSDMD), whose N-terminal domain inserts into the cell membrane to form pores, leading to pyroptotic cell death. Activated GSDMD can also accumulate in the mitochondrial membrane, triggering ROS production and the formation of mitochondrial pores, resulting in the release of mtDNA into the cytoplasm, where it is recognized by cytoplasmic mitochondrial sensors.[30] Secondly, excessive ROS can activate several inflammatory signaling pathways, including JNK, which induces apoptosis and autophagy.[18,31] JNK activation can stimulate the NF-κB pathway, increasing the expression of pro-inflammatory cytokines, triggering inflammation and activating downstream genes, ultimately causing cellular damage[18,19] Established literature shows that the activated NF-κB pathway can cause liver damage and cholestasis by inhibiting FXR and LXR expression,[17,32] which represses downstream bile acid and sterol transporter genes. Furthermore, NF-κB is known to interact with the JNK/c-Jun signaling pathway.[33] Our findings build directly on this knowledge, showing that MRPL35 overexpression decreases ROS production and the subsequent activation of both the JNK and NF-κB pathways. This positions MRPL35 as a key upstream regulator that can control the ROS-JNK-NF-κB signaling axis, thereby influencing both inflammation and bile acid transport in PNAC pathogenesis.

Limitations

Several limitations should be acknowledged. First, the small clinical sample size (n=10 for PNAC, n=13 for control) may limit the generalizability of our findings, necessitating validation in larger multicenter cohorts. Second, using exclusively male rats may introduce gender bias, as sexual dimorphism in hepatic metabolism could influence MRPL35 function and therapeutic responses. Third, the absence of loss-of-function experiments (siRNA or CRISPR knockdown) and comprehensive mitochondrial functional assessments (oxygen consumption, ATP production, membrane potential) limits mechanistic conclusions. Fourth, adenoviral vector limitations, including transient expression and potential immunogenicity, may affect long-term outcomes and clinical translation. Fifth, the upstream mechanisms regulating MRPL35 downregulation remain undefined. Sixth, the absence of a control group treated with N-acetylcysteine (NAC) alone makes it difficult to differentiate the specific effects of MRPL35 restoration from a general antioxidant response. Finally, while our preclinical findings are promising, translation to clinical practice will require alternative approaches such as small molecule modulators or repurposed drugs, as gene therapy in neonates faces substantial regulatory and safety challenges.

Conclusion

In conclusion, this study demonstrates that MRPL35 downregulation contributes to PNAC pathogenesis by activating the ROS/JNK/NF-κB signaling cascade. In our experimental model, restoring MRPL35 expression attenuated hepatic inflammation, oxidative stress, and liver injury, an effect that was enhanced by co-treatment with an antioxidant.

These findings identify the MRPL35-mediated mitochondrial-inflammation axis as a promising therapeutic target for neonates with PNAC.

Institutional Review Board Statement

The study was conducted in accordance with the Declaration of Helsinki, and approved by the Institutional Review Board of Institutional Ethics Review Board of the First Affiliated Hospital of Army Medical University, China (KY2021050, 2021-08-02). The animal study protocol was approved by the Institutional Review Board of Ethics Committee of the Army Medical University, China (AMUWEC20201551).

Abbreviations

ALT, Alanine aminotransferase; AST, Aspartate aminotransferase; DBil, Direct Bilirubin; ELISA, Enzyme-linked immunosorbent assay; FXR, Farnesoid X receptor; GGT, gammaglutamyl transferase; HE, Hematoxylin-Eosin; IL-10, Interleukin-10; IL-1β, Interleukin-1 beta; IL-4, Interleukin-4; JNK, c-Jun N-terminal kinase; LXR, liver X receptors; MDA, Malondialdehyde; MRPL35, Mitochondrial ribosomal protein L35; NAC N-acetylcysteine; NF-κB, Nuclear factor-kappa B; PBMC, Peripheral Blood Mononuclear Cell; PNAC, Parenteral nutrition associated cholestasis; qRT-PCR, Quantitative Real-time PCR; ROS, Reactive oxygen species; TBA, Total bile acid; TBil, Total bilirubin; TNF-α, Tumor Necrosis Factor-alpha; WB, Western Blot.

Data Sharing Statement

Data are contained within the article. The data underlying this article will be shared on reasonable request to the corresponding author. Raw data files including Western blot images, flow cytometry data, and statistical analyses are available in the supplementary materials.

Informed Consent Statement

Informed consent was obtained from all subjects involved in the study. Written informed consent has been obtained from the parents or legal guardians to publish this paper.

Acknowledgments

The authors would like to express their gratitude to EditSprings (https://www.editsprings.cn) for the expert linguistic services provided. We also thank the nursing staff of the NICU for their assistance in sample collection and the pathology department for histological analyses.

Author Contributions

All authors made a significant contribution to the work reported, whether that is in the conception, study design, execution, acquisition of data, analysis and interpretation, or in all these areas; took part in drafting, revising or critically reviewing the article; gave final approval of the version to be published; have agreed on the journal to which the article has been submitted; and agree to be accountable for all aspects of the work.

Funding

This research was funded by National Natural Science Foundation of China (Nos. 82170565). Special project to improve scientific and technological innovation capabilities of Army Medical University (Nos. 2019XQY09). Army Medical University Excellent Talent Pool Key Support Program Project (Nos. XZ-2019-505-030).

Disclosure

The authors declare no conflicts of interest.

References

1. Tume LN, Valla FV, Joosten K, et al. Nutritional support for children during critical illness: European society of pediatric and neonatal intensive care (ESPNIC) metabolism, endocrine and nutrition section position statement and clinical recommendations. *Intensive Care Med*. 2020;46(3):411–425. doi:10.1007/s00134-019-05922-5
2. Khalaf RT, Sokol RJ. New insights into intestinal failure-associated liver disease in children. *Hepatology*. 2020;71(4):1486–1498. doi:10.1002/hep.31152
3. Lauriti G, Zani A, Aufieri R, et al. Incidence, prevention, and treatment of parenteral nutrition-associated cholestasis and intestinal failure-associated liver disease in infants and children: a systematic review. *JPEN J Parenter Enteral Nutr*. 2014;38(1):70–85. doi:10.1177/0148607113496280
4. Guthrie G, Burrin D. Impact of parenteral lipid emulsion components on cholestatic liver disease in neonates. *Nutrients*. 2021;13(2):508. doi:10.3390/nu13020508
5. Ghosh S, Devereaux MW, Anderson AL, et al. NF-κB regulation of LRH-1 and ABCG5/8 potentiates phytosterol role in the pathogenesis of parenteral nutrition-associated cholestasis. *Hepatology*. 2021;74(6):3284–3300. doi:10.1002/hep.32071
6. El Kasmi KC, Ghosh S, Anderson AL, et al. Pharmacologic activation of hepatic farnesoid X receptor prevents parenteral nutrition-associated cholestasis in mice. *Hepatology*. 2022;75(2):252–265. doi:10.1002/hep.32101
7. Miao J, Choi SE, Seok SM, et al. Ligand-dependent regulation of the activity of the orphan nuclear receptor, small heterodimer partner (SHP), in the repression of bile acid biosynthetic CYP7A1 and CYP8B1 genes. *Mol Endocrinol*. 2011;25(7):1159–1169. doi:10.1210/me.2011-0033
8. Pietromonaco SF, Denslow ND, O'Brien TW. Proteins of mammalian mitochondrial ribosomes. *Biochimie*. 1991;73(6):827–835. doi:10.1016/0300-9084(91)90062-6
9. Box JM, Kaur J, Stuart RA. MrpL35, a mitospecific component of mitoribosomes, plays a key role in cytochrome c oxidase assembly. *Mol Biol Cell*. 2017;28(24):3489–3499. doi:10.1091/mbc.E17-04-0235
10. Zhang L, Lu P, Yan L, et al. MRPL35 is up-regulated in colorectal cancer and regulates colorectal cancer cell growth and apoptosis. *Am J Pathol*. 2019;189(5):1105–1120. doi:10.1016/j.ajpath.2019.02.003
11. Bae JH, Jo SI, Kim SJ, et al. Circulating cell-free mtDNA contributes to AIM2 inflammasome-mediated chronic inflammation in patients with type 2 diabetes. *Cells*. 2019;8(4):328. doi:10.3390/cells8040328
12. Karthigesu K, Bertolo RF, Brown RJ. Parenteral nutrition and oxidant load in neonates. *Nutrients*. 2021;13(8):2631. doi:10.3390/nu13082631
13. Feldman AG, Sokol RJ. Neonatal cholestasis: updates on diagnostics, therapeutics, and prevention. *Neoreviews*. 2021;22(12):e819–e836. doi:10.1542/neo.22-12-e819
14. Jackson RL, White PZ, Zalla J. SMOFlipid vs intralipid 20%: effect of mixed-oil vs soybean-oil emulsion on parenteral nutrition-associated cholestasis in the neonatal population. *JPEN J Parenter Enteral Nutr*. 2021;45(2):339–346. doi:10.1002/jpen.1843
15. Hodin CM, Visschers RG, Rensen SS, et al. Total parenteral nutrition induces a shift in the firmicutes to bacteroidetes ratio in association with paneth cell activation in rats. *J Nutr*. 2012;142(12):2141–2147. doi:10.3945/jn.112.162388
16. Pang D, Laferriere C. Review of intraperitoneal injection of sodium pentobarbital as a method of euthanasia in laboratory rodents. *J Am Assoc Lab Anim Sci*. 2020;59(3):346. doi:10.30802/AALAS-JAALAS-19-000081
17. El Kasmi KC, Vue PM, Anderson AL, et al. Macrophage-derived IL-1β/NF-κB signaling mediates parenteral nutrition-associated cholestasis. *Nat Commun*. 2018;9(1):1393. doi:10.1038/s41467-018-03764-1
18. Mihajlovic M, Rosseel Z, De Waele E, et al. Parenteral nutrition-associated liver injury: clinical relevance and mechanistic insights. *Toxicol Sci*. 2024;199(1):1–11. doi:10.1093/toxsci/kfae020
19. Yahfoufi N, Alsadi N, Jambi M, et al. The Immunomodulatory and anti-inflammatory role of polyphenols. *Nutrients*. 2018;10(11):1618. doi:10.3390/nu10111618
20. Orso G, Mandato C, Veropalumbo C, et al. Pediatric parenteral nutrition-associated liver disease and cholestasis: novel advances in pathomechanisms-based prevention and treatment. *Dig Liver Dis*. 2016;48(3):215–222. doi:10.1016/j.dld.2015.11.003
21. Zhang Z, Sun J, Jin C, et al. Identification and validation of a fatty acid metabolism gene signature for the promotion of metastasis in liver cancer. *Oncol Lett*. 2023;26(4):457. doi:10.3892/ol.2023.14044
22. Lavoie JC, Chessex P. Parenteral nutrition and oxidant stress in the newborn: a narrative review. *Free Radic Biol Med*. 2019;142:155–167. doi:10.1016/j.freeradbiomed.2019.02.020
23. Lopez Sanchez MIG, Krüger A, Shiriaev DI, et al. Human mitoribosome biogenesis and its emerging links to disease. *Int J Mol Sci*. 2021;22(8):3827. doi:10.3390/ijms22083827
24. Gopisetty G, Thangarajan R. Mammalian mitochondrial ribosomal small subunit (MRPS) genes: a putative role in human disease. *Gene*. 2016;589(1):27–35. doi:10.1016/j.gene.2016.05.008
25. Box JM, Anderson JM, Stuart RA. Mutation of the PEBP-like domain of the mitoribosomal MrpL35/mL38 protein results in production of nascent chains with impaired capacity to assemble into OXPHOS complexes. *Mol Biol Cell*. 2023;34(13):ar131. doi:10.1091/mbc.E23-04-0132
26. Ghosh S, Devereaux MW, Liu C, Sokol RJ. LRH-1 agonist DLPC through STAT6 promotes macrophage polarization and prevents parenteral nutrition-associated cholestasis in mice. *Hepatology*. 2024;79(5):986–1004. doi:10.1097/HEP.0000000000000690
27. Tait SW, Green DR. Mitochondrial regulation of cell death. *Cold Spring Harb Perspect Biol*. 2013;5(9):a008706. doi:10.1101/cshperspect.a008706
28. Rongvaux A, Jackson R, Harman CC, et al. Apoptotic caspases prevent the induction of type I interferons by mitochondrial DNA. *Cell*. 2014;159(7):1563–1577. doi:10.1016/j.cell.2014.11.037
29. White MJ, McArthur K, Metcalf D, et al. Apoptotic caspases suppress mtDNA-induced STING-mediated type I IFN production. *Cell*. 2014;159(7):1549–1562. doi:10.1016/j.cell.2014.11.036
30. Huang LS, Hong Z, Wu W, et al. mtDNA activates cGAS signaling and suppresses the YAP-mediated endothelial cell proliferation program to promote inflammatory injury. *Immunity*. 2020;52(3):475–486.e5. doi:10.1016/j.immuni.2020.02.004
31. Liu X, Zhao P, Wang X, et al. Celastrol mediates autophagy and apoptosis via the ROS/JNK and Akt/mTOR signaling pathways in glioma cells. *J Exp Clin Cancer Res*. 2019;38(1):184. doi:10.1186/s13046-019-1173-4
32. Cai SY, Ouyang X, Chen Y, et al. Bile acids initiate cholestatic liver injury by triggering a hepatocyte-specific inflammatory response. *JCI Insight*. 2017;2(5):e90780. doi:10.1172/jci.insight.90780
33. De Smaele E, Zazzeroni F, Papa S, et al. Induction of gadd45beta by NF-kappaB downregulates pro-apoptotic JNK signalling. *Nature*. 2001;414(6861):308–313. doi:10.1038/35099560